Closure of parallel cracks: Micromechanical estimates versus finite element computations

Joffrey Bluthé, Benoît Bary, Éric Lemarchand

Closure of parallel cracks: micromechanical estimates versus finite element computations

Joffrey Bluthé[a,b,*], Benoît Bary[a], Eric Lemarchand[b]

[a]*Den-Service d'Etude du Comportement des Radionucléides (SECR), CEA, Université de Paris- Saclay, F-91191, France*
[b]*Laboratoire Navier - UMR 8205, CNRS, École des Ponts ParisTech, France*

Abstract

3D finite element simulations have been performed in order to assess the ability of four classical homogenization schemes to model the elastic behavior of solids with parallel cracks, namely the dilute, Mori-Tanaka, self-consistent and differential schemes. The cracks have been represented by right circular cylinders with aspect ratios as low as 10^{-3} in the simulations whose centroids are randomly located in the REV. Special attention has been paid to the crack aspect ratio variation predicted by the different schemes, since the goal is ultimately to propose a non-linear micromechanical model of a cracked solid, taking complete crack closure into account.

The results confirm earlier studies which showed that the differential scheme was best suited for this kind of morphology when computing elastic moduli, but additionally, we show that changes in crack aperture are also accurately predicted. It is however noted that the randomness in the positions of the cracks leads to significant scatter in the magnitude of the aperture variation inside a given simulation, which suggests that the cracks do not close simultaneously. As a consequence, non-linear numerical simulations accounting for contact between the crack lips should be performed in order to completely validate a non-linear micromechanical model in alternate tension/compression loading cases.

Keywords: Cracked media, strain concentration, crack closure, numerical simulations, homogenization theory

1. Introduction

Every solid body can be seen as composite at some scale, with the exception of the single crystal solid. This trivial observation explains the strong interest in the determination of effective properties of heterogeneous systems developed in the past century. Several different strategies exist to undertake this challenging task. In the present paper, Eshelby-based micromechanics arguments and numerical tools are both derived. The first one is based on Eshelby's solution to the problem of a single ellipsoidal inclusion embedded in an infinite medium (Eshelby [11]); this method has

*Corresponding author
Email address: bluejof@gmail.com (Joffrey Bluthé)

the advantage of being often completely analytical, which is interesting for parametric analysis. Its main drawback is that a fair number of simplifying assumptions usually have to be introduced in order to conduct any calculation to the end, which may limit its range of applicability. The second method relies entirely on numerical tools and is one of brute force; it consists in generating the desired microstructures and in performing numerical experiments on said structures, using some finite element software. The main advantages of the second method are that its implementation is straightforward, that much more complex and realistic geometries can be investigated, and that it gives access to local information in the multiple phases considered instead of just average quantities. However, it may require a high computing power. Even creating the geometry can prove to be very challenging for current softwares, especially in a periodic context, and the resulting mesh is not always satisfactory, particularly when dealing with singular geometries such as crack tips. That being said, the recent advances in computer technology have made this method more and more available to researchers, and it is an interesting tool to investigate the consistency of analytical estimates.

One area of particular interest for many applications is the behavior of cracked rocks. A number of researchers have applied the tools of micromechanics to determine the behavior of cracked media in order to account for a coherent coupling between their mechanical behavior and their transport properties. This approach has been implemented in Dormieux and Kondo [9] to estimate both the effective stiffness and hydraulic conductivity of rocks in the context of the self-consistent approximation, whereby the cracks of ellipsoidal shape are endowed with a fictitious permeability derived from a Poiseuille law in order to reduce the problem to a conductivity homogenization procedure. The resulting effective hydraulic conductivity is a function of both the aspect ratio of the cracks X and their uniform radius a, which allows the authors to take into account the impact of both crack propagation and crack opening/closure on the homogenized transport properties. These ideas were further investigated by Barthélémy [1], who considered the presence of cracks at two different scales and studied the differences between their respective mathematical treatments, and by Lemarchand et al. [20] and Lemarchand et al. [21]; in a similar approach, Vu et al. [29] proposed to model the impact of crack propagation on the effective permeability; finally, Levasseur et al. [22] built on Dormieux and Kondo [9] in order to predict the permeability change related to damage caused by an excavation process. Following the latter, the same kind of methodology can be applied to the opposite process, i.e. permeability reduction caused by the mechanical closure of fractures during the service life of a drift. A first attempt was made in Bluthé et al. [4], who proposed an estimate of the crack closure due to either an applied mechanical load or a hydration-induced swelling process in the context of the Mori-Tanaka approximation. Restricted to a linear context, the latter is currently being extended to the non-linear case associated with the complete crack closure. Complete closure is indeed expected because of radial compression due to the swelling of both the clay core and that of the damaged zone (see Bluthé et al. [4]).

The extension to non-linearity is entirely possible without much difficulty, since the theoretical background was laid out by Deude et al. [8]. In this work, the average crack closure is estimated in the context of the Mori-Tanaka scheme by using the strain concentration rule in the cracks in the limit of infinitesimal aspect ratios $X \ll 1$, and the closure criterion reduces to $\Delta X < -X_0$, where X_0 is the initial aspect ratio of the crack and $\Delta X = X - X_0$. The effective tangent stiffness of the cracked medium is then computed as a function of which crack families are still open. Since the

set of closed crack families is itself a function of the current stress state, the effective mechanical behavior of the medium is indeed non-linear. However, for such an approach to be valid, use of a particular micromechanical scheme requires it to predict accurately both the effective stiffness and the crack closure. Since the homogenization schemes rely on the estimation of the average strain concentration tensors in the different phases, one could be tempted to imagine that hypotheses that lead to good stiffness predictions might also lead to good strain concentration predictions. To the author's knowledge, this has not received much attention in the past, so this paper mainly aims at contributing on this aspect. Thus, the goal of this work is to identify a relevant homogenization scheme in terms of both the effective stiffness and the crack aperture changes during loading, in order to later use the selected scheme in a non-linear mechanical model at the scale of a structure, similarly to what can be found in the linear case in Bluthé et al. [4].

Let us first summarize briefly the literature on the confrontation of the standard micromechanical schemes with numerical simulations for cracked media. In some of the cases cited below, the authors studied both the case of randomly oriented cracks and that of parallel cracks, but we will restrict our discussion to the latter case since this is the context of the present study. The first attempts can be traced back to the mid 1990s when Huang et al. [17] implemented three of the most used micromechanical schemes, namely the dilute scheme, the differential scheme and the self-consistent scheme, for an elastic solid containing parallel cracks, and assessed their performance in comparison with 2D numerical simulations performed by applying the boundary element method (BEM) to a unit cell containing 25 cracks. For each value of the crack density parameter ϵ, as introduced in Budiansky and O'connell [5], the authors generated 15 different crack distributions, which allowed for an estimation of the variability in their computation. In the studied range of crack densities, namely from 0.1 to 0.6, their numerical results lie between the dilute and the differential approximations. A few years later, Zhan et al. [31] performed the same kind of numerical experiments but with another method, this time based on Muskelishvili's complex potentials. Again, their results seem to lie between the differential and the dilute approximation, but one of the numerical methods lies closer to the dilute estimate. This point, which may seem quite odd at first sight since the dilute estimate neglects any interaction between the cracks, will be discussed in section 2.2. Dahm and Becker [7] used both the finite element method (FEM) and the BEM to numerically compute the effective moduli of different crack distributions in 2D and found the differential estimate to fit the results better than the dilute estimate. Orlowsky et al. [23] confirmed this result by simulating elastic wave propagation, still in 2D. Shen and Li [27] further established the good performances of the differential scheme using Kachanov's approximate method to solve their system of integral equations (Kachanov [18]). However, they pointed out that the discrepancy becomes significant for crack densities above 0.4. Saenger et al. [25] and Saenger et al. [26] used the so-called rotated staggered grid technique to evaluate the dynamic response of cracked rocks in 3D, and their static response in 2D in the context of either uniform displacement or uniform stress conditions. The authors used this technique to explain the scatter on the numerical estimates of the moduli found in the literature and concluded that the differential scheme could not be set aside by any of the analyzed previous results. However, further 3D finite element estimates given by Grechka [12] tend to favor the dilute scheme with respect to the differential scheme (see discussion below). Note that for these numerical computations, the cracks were modeled as spheroids of aspect ratio 0.08. More recently, Charpin and Ehrlacher

[6] proposed to evaluate the relevance of additional schemes in 2D, namely the interaction direct derivative estimate (IDD, see Zheng and Du [32]) and its modified version named full-range IDD (FRIDD), based on a comparison with finite element computations performed on periodic cells containing elliptical holes with an aspect ratio of either 0.1 or 0.01. The authors concluded that the FRIDD method was good at estimating the poromechanical properties of cracked media, but it should be noted that the presented results did not include the differential estimate. Finally, the most recent results are due to Vasylevskyi et al. [28], who performed 3D finite element calculations on 3D periodic cells of ellipsoids with an aspect ratio of 0.01 embedded in an orthotropic matrix. Here, the authors identified the differential scheme as giving the best results for out-of-plane moduli, and the Mori-Tanaka scheme for the in-plane ones. However, as pointed out by the authors, in the limit of infinitely flat spheroids the presence of these cavities does not impact the in-plane moduli, so that these results do not appear particularly relevant for choosing the appropriate scheme.

In this paper, we propose to investigate further the performance of five classical homogenization schemes in comparison with finite element simulations on periodic representative elementary volumes. As mentioned above, special attention was paid to variations in crack apertures upon loading. First, the main analytical results are recalled for the chosen approximations, namely the dilute, Mori-Tanaka, self-consistent and differential schemes and the Ponte-Castaneda and Willis bound. Both the compliance tensors and crack aperture variations are derived in all cases, and a few necessary comments on the range of applicability of the dilute scheme are made. Then, the numerical simulations are described: we specify the geometries and how they were generated, we explain how the boundary conditions and mesh size were chosen, and assess the quality of our results. Finally, the numerical results are presented and discussed, and we propose perspectives for future works.

2. Analytical estimates

2.1. General strategy

Consider a representative elementary volume (REV) Ω of a cracked solid with aligned parallel cracks. From a micromechanical point of view, cracks are usually assumed to be oblate spheroidal cavities—meaning that they are treated as spheroidal inclusions with volume fraction $f = \frac{4\pi}{3}\mathcal{N}a^2c$, where $\mathcal{N}$ is the number of cracks per unit volume of REV and a and c are the semi-major and semi-minor axes of the oblate spheroids respectively (see figure 1)—with a vanishing stiffness tensor ($\mathbb{C}^c \to 0$), assumed isotropic for simplicity. Here, all the cavities are additionally assumed to be self-similar. The solid matrix itself has a volume fraction $1 - f$ and the stiffness tensor $\mathbb{C}^m$. The general strategy for the determination of the strain-based estimates of the effective stiffness and of the crack aperture variation Δc is briefly recalled, following Dormieux and Kondo [10].

Uniform strain boundary conditions are here applied to the composite, i.e. $\xi(\boldsymbol{z}) = \boldsymbol{E}\cdot\boldsymbol{z}$ is applied on the boundary $\partial\Omega$ of the REV, where $\boldsymbol{z}$ denotes the position vector within the REV. As long as the geometry is not singular, the strain tensor at any point $\boldsymbol{z}$ of the composite depends linearly on the loading parameter $\boldsymbol{E}$ through the fourth-rank concentration tensor, i.e. $\boldsymbol{\varepsilon}(\boldsymbol{z}) = \mathbb{A}(\boldsymbol{z}) : \boldsymbol{E}$. Here and in the following developments, the colon denotes the standard double contraction of tensors. Note that the strain average rule $\overline{\boldsymbol{\varepsilon}} = \boldsymbol{E}$ implies that $f\overline{\mathbb{A}}^c + (1-f)\overline{\mathbb{A}}^m = \mathbb{I}$, where the following

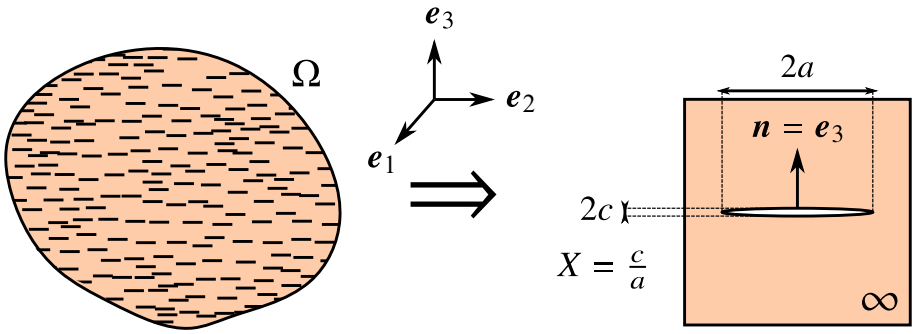

Figure 1: Cracked solid Ω (left) and representation of the auxiliary problem (right).

averaging operators have been introduced:

$$\overline{\boldsymbol{\varepsilon}} = \frac{1}{|\Omega|}\int_{\Omega} \boldsymbol{\varepsilon}(z)\,\mathrm{d}V; \quad \overline{\mathbb{A}}^{\alpha} = \frac{1}{|\Omega_\alpha|}\int_{\Omega_\alpha} \mathbb{A}(z)\,\mathrm{d}V \quad (\alpha = c \text{ or } m) \tag{1}$$

and Ω_c and Ω_m denote the crack domain and the solid domain respectively. It then follows from the local constitutive equation of linear elasticity $\boldsymbol{\sigma}(z) = \mathbb{C}(z) : \boldsymbol{\varepsilon}(z)$ that the average stress is linearly related to the average strain, so that the homogenized stiffness tensor $\mathbb{C}^{hom}$ may be defined as:

$$\boldsymbol{\Sigma} = \overline{\boldsymbol{\sigma}} = \mathbb{C}^{hom} : \boldsymbol{E}; \quad \mathbb{C}^{hom} = \overline{\mathbb{C}(z) : \mathbb{A}(z)} \tag{2}$$

Using this definition, we obtain the relationship between $\mathbb{C}^{hom}$ and $\overline{\mathbb{A}}^{c}$:

$$\mathbb{C}^{hom} = \mathbb{C}^{m} + f(\mathbb{C}^{c} - \mathbb{C}^{m}) : \overline{\mathbb{A}}^{c} \tag{3}$$

Introducing the crack density parameter $\epsilon = \mathcal{N}a^3$ (Budiansky and O'connell [5]) and the aspect ratio of the cracks $X = \frac{c}{a}$, the crack volume fraction reads $f = \frac{4\pi}{3}\epsilon X$, so that (3) yields:

$$\mathbb{C}^{hom} = \mathbb{C}^{m} : \left(\mathbb{I} - \frac{4\pi}{3}\epsilon X \overline{\mathbb{A}}^{c}\right) \tag{4}$$

Within the considered assumptions, (4) is an exact definition of the homogenized stiffness. This exact definition cannot be used as such in practice, but the tools of micromechanics yield approximations through estimates of the average concentration tensor $\overline{\mathbb{A}}^{c}$ over the crack domain. Note that technically speaking, the previous analysis should be performed in the rate form because cracks satisfy the condition $X \ll 1$ and therefore undergo large strains. However, as explained in Dormieux and Kondo [10], under this very condition $X\overline{\mathbb{A}}^{c}$ may be replaced by its limit as $X \to 0$, so that the non-linearity disappears and the previous developments do hold.

The average increment of aspect ratio upon loading may then be computed:

$$\frac{c - c_0}{c} = \frac{\Delta c}{c} = (\boldsymbol{n} \otimes \boldsymbol{n}) : \overline{\boldsymbol{\varepsilon}}^{c} \tag{5}$$

where $\boldsymbol{n}$ is the unit normal to the midplane of the crack and c_0 is the value of c in the reference configuration. This quantity is singular as $X \to 0$, but for non-propagating cracks (constant a), the average increment of aspect ratio is regular and is obtained using the strain concentration rule:

$$\Delta X = \frac{\Delta c}{a} = (\boldsymbol{n} \otimes \boldsymbol{n}) : \left(X \overline{\mathbb{A}}^{c} \right) : \mathbb{S}^{hom} : \boldsymbol{\Sigma} \tag{6}$$

Taking advantage of (4), it is convenient to express (6) in terms of $\mathbb{S}^{hom}$ alone:

$$\Delta X = \frac{3}{4\pi\epsilon} (\boldsymbol{n} \otimes \boldsymbol{n}) : \left(\mathbb{S}^{hom} - \mathbb{S}^{m} \right) : \boldsymbol{\Sigma} \tag{7}$$

which holds for any scheme and is especially convenient when the compliance tensor of the effective medium is known. It is straightforward to deduce from (7) that ΔX will be independent of ϵ for any scheme that predicts an affine dependence of $\mathbb{S}^{hom}$ on ϵ.

Estimates of the concentration tensor $\overline{\mathbb{A}}^{c}$ now have to be proposed in order to make quantitative predictions of the homogenized stiffness. All the analytical micromechanical estimates are based on Eshelby's solution to the so-called transformation problem of an infinite elastic medium with stiffness tensor $\mathbb{C}^0$ with a region subjected to a uniform eigenstrain (Eshelby [11]). According to this result, the strain in a single spheroidal cavity embedded in an infinite matrix which is subjected to uniform strain boundary conditions $\xi(\boldsymbol{z}) = \boldsymbol{E}^0 \cdot \boldsymbol{z}$ at infinity is uniform in the inclusion and given by:

$$\boldsymbol{\varepsilon}^{c} = \left(\mathbb{Q}^{c,0} \right)^{-1} : \mathbb{C}^0 : \boldsymbol{E}^0; \quad \mathbb{Q}^{c,0} = \mathbb{C}^0 - \mathbb{C}^0 : \mathbb{P}^{c,0} : \mathbb{C}^0 \tag{8}$$

where the Hill tensors of the crack $\mathbb{P}^{c,0}$ and $\mathbb{Q}^{c,0}$ have been introduced. Both of these tensors are functions of the shape of the crack (superscript c) and of the stiffness tensor $\mathbb{C}^0$ of the reference medium (superscript 0). Following the classical nomenclature (see Hill [14]), we will refer to this problem as the auxiliary problem; its solution is then used to estimate the average strain in the inclusion phase for the actual problem defined above on the composite. This is done by proposing adequate values for $\boldsymbol{E}^0$ and $\mathbb{C}^0$.

2.2. Dilute scheme

In the dilute approximation, the interaction between the cracks is neglected, which means that each inclusion only "sees" the infinite matrix. This is obtained by setting $\mathbb{C}^0 = \mathbb{C}^m$ and $\boldsymbol{E}^0 = \boldsymbol{E}$ in (8), so that $\overline{\mathbb{A}}^{c} = (\mathbb{Q}^{c,m})^{-1} : \mathbb{C}^m$. Denoting $\mathbb{U}^{c,m} = \lim_{X \to 0} X \, (\mathbb{Q}^{c,m})^{-1}$, the following estimate for the effective compliance tensor is obtained:

$$\mathbb{S}^{hom} \sim \mathbb{S}^{dil} = \mathbb{S}^{m} + \frac{4\pi}{3} \epsilon \mathbb{U}^{c,m} \tag{9}$$

This form together with (A.2) make it clear that only the out-of-plane Young's modulus and shear modulus are affected, which will be true of all the schemes. These moduli are given by:

$$\begin{cases} \dfrac{E_3^{hom}}{E} \sim \dfrac{E_3^{dil}}{E} = 1 - \dfrac{16}{3}(1 - \nu^2)\epsilon \\ \dfrac{\mu_{13}^{hom}}{\mu} \sim \dfrac{\mu_{13}^{dil}}{\mu} = 1 - \dfrac{16}{3} \dfrac{1-\nu}{2-\nu} \epsilon \end{cases} \tag{10}$$

where E, μ and ν are the Young's modulus, shear modulus and Poisson's ratio of the isotropic matrix. This result is obtained by expansion to first order in ϵ, because of the assumption of dilution.

Using (7) and (9), we get the average increment of aspect ratio:

$$\Delta X^{dil} = U^{c,m}_{3333}\Sigma_{33} \tag{11}$$

2.3. Mori-Tanaka scheme

The Mori-Tanaka scheme is a first relevant candidate to take some interaction between the cracks into account. It is based on the assumption that each inclusion is embedded in the actual matrix, so that $\mathbb{C}^0 = \mathbb{C}^m$, but that the composite with a single inclusion is subjected to the average strain in the matrix so that $\boldsymbol{E}^0 = \overline{\boldsymbol{\varepsilon}}^m$. Using the strain average rule to determine $\boldsymbol{E}^0$ as a function of $\boldsymbol{E}$, the following estimate of the effective compliance tensor is obtained:

$$\mathbb{S}^{hom} \sim \mathbb{S}^{MT} = \mathbb{S}^m + \frac{4\pi}{3}\epsilon\mathbb{U}^{c,m} \tag{12}$$

This is formally equivalent to (9), but there is no need for an expansion to first order in ϵ this time, so that the effective moduli read:

$$\begin{cases} \frac{E_3^{hom}}{E} \sim \frac{E_3^{MT}}{E} = \left(1 + \frac{16}{3}(1-\nu^2)\epsilon\right)^{-1} \\ \frac{\mu_{13}^{hom}}{\mu} \sim \frac{\mu_{13}^{MT}}{\mu} = \left(1 + \frac{16}{3}\frac{1-\nu}{2-\nu}\epsilon\right)^{-1} \end{cases} \tag{13}$$

Since the compliance estimates are identical, (7) shows that the Mori-Tanaka estimate of average increment of aspect ratio is given by (11).

2.4. Self-consistent scheme

It is usually considered that the Mori-Tanaka scheme can only take into account a limited amount of interaction between the inclusions. Stronger interactions can be obtained in other ways, the first of which is the self-consistent approximation. It consists in assuming that each crack is embedded in the sought homogenized medium itself, i.e. $\mathbb{C}^0 = \mathbb{C}^{hom} \simeq \mathbb{C}^{sc}$, which yields an implicit equation for $\mathbb{C}^{sc}$. Different kinds of self-consistent estimates exist in the literature, but for simplicity we chose to follow Hashin [13] and treated the composite as a dispersion in the present study, leading to the following implicit equation for the effective compliance:

$$\mathbb{S}^{sc} = \mathbb{S}^m + \frac{4\pi}{3}\epsilon\mathbb{U}^{c,sc} \tag{14}$$

Note the fundamental difference between (12) and (14) which lies in the superscripts, so that (14) does not give the homogenized compliance explicitly. This implicit equation is easily solved for E_3^{sc} and μ_{13}^{sc} numerically using a standard software.

Once the homogenized stiffness is known, the average increment of aspect ratio can be computed using (7) and (14):

$$\Delta X^{sc} = U^{c,sc}_{3333}\Sigma_{33} \tag{15}$$

2.5. Differential scheme

As mentioned in Hashin [13], the main criticism of the self-consistent scheme is the existence of a so-called percolation threshold for certain kinds of porous media, that is, a certain finite porosity or crack density for which $\mathbb{C}^{sc}$ is no longer positive definite. It is the case for spherical voids as well as randomly oriented penny-shaped cracks, and may be inaccurate since it seems to contradict several experimental results. The differential scheme has been proposed to account for a strong interaction between the cracks without percolation effects. It consists in building the cracked material incrementally by adding an infinitesimal amount of cracks to the material, until the desired crack density is reached. This process leads to the following differential equation for the effective compliance:

$$\frac{\mathrm{d}}{\mathrm{d}e}\mathbb{S}^{dif} = \frac{4\pi}{3}\mathbb{U}^{c,dif} \tag{16}$$

This differential equation is easily solved for E_3^{dif} and μ_{13}^{dif} numerically using a standard software.

The average increment of aspect ratio is then obtained using (7). It is interesting to note that since $\frac{1}{\epsilon}\left(\mathbb{S}^{dif} - \mathbb{S}^{m}\right)$ is the mean value of $\frac{\mathrm{d}}{\mathrm{d}e}\mathbb{S}^{dif}(e)$ over $[0, \epsilon]$, which is given by (16), we also have the following result:

$$\Delta X^{dif} =< U_{3333}^{c,dif} > \Sigma_{33} \tag{17}$$

with $< \bullet >= \frac{1}{\epsilon}\int_0^{\epsilon} \bullet \, \mathrm{d}e$.

2.6. Pont-Castaneda and Willis bound

Another class of estimates may be obtained from the Hashin-Shtrikman variational principles. Details can be found in Ponte Castaneda and Willis [24], but the main points are first that they are functions of the spatial distribution of the inclusion phase in the composite, and secondly that these are explicit under the assumption of ellipsoidal symmetry of the distribution. The two simplest cases are obtained when the distribution is either spherical, or defined by the shape of the inclusions themselves. As is well known, the latter case reduces to the Mori-Tanaka estimate, and will not be discussed further, while the former case leads to the following estimates:

$$\begin{cases} \frac{E_3^{hom}}{E} \sim \frac{E_3^{PCW}}{E} = 1 - \frac{240\epsilon(1-\nu^2)}{45+16\epsilon(7-15\nu^2)} \\ \frac{\mu_{13}^{hom}}{\mu} \sim \frac{\mu_{13}^{PCW}}{\mu} = 1 - \frac{240\epsilon(1-\nu)}{45(2-\nu)+32\epsilon(4-5\nu)} \end{cases} \tag{18}$$

Again, the average increment of aspect ratio is obtained using (7). An interesting feature of these estimates is that these are rigorous upper bounds for composites satisfying the spatial distribution requirements in a certain range for ϵ, which is why they are often referred to as the Ponte-Castaneda and Willis (PCW) bounds. For example, (18) are rigorous upper bounds for the out-of-plane moduli of a composite with parallel cracks and a spherical distribution in the range $0 \leq \epsilon \leq \frac{3}{4\pi}$. Finally, one should note that the effective Young's modulus and shear modulus vanish for $\epsilon = \frac{45}{128}$ and $\epsilon = \frac{45(2-\nu)}{16(7-5\nu)}$, so that they do not cover the whole range of values studied here numerically (see section 3).

3. Numerical simulations

Let us now turn to the numerical simulations that we performed in order to assess the performance of the previously described homogenization scheme. Although the goal is eventually to propose a non-linear model accounting for complete crack closure during compression of a cracked rock, the simulations performed here remain in a completely linear context. The effective out-of-plane Young's modulus and increment of crack aspect ratio were determined by applying a uniaxial tension to the elementary volumes so that the cracks tend to open instead of close, but compression would only reverse the sign because of linearity.

3.1. Preliminary investigations

First, let us describe the procedures used to generate the volume elements and to assess the validity of the numerical approach. The sample generation procedure is based on a random distribution of inclusion centroids of prescribed shape and size in a box, and has been applied to various studies and contexts, see e.g. Bary et al. [2], Honorio et al. [16] and Bary et al. [3]. It makes use of the python tool Combs developed in the framework of the CAD platform Salome[1]. In the present paper, following Charpin and Ehrlacher [6] and Vasylevskyi et al. [28], it was decided to introduce cracks with a shape approaching the one considered in the analytical developments, i.e. with a non-zero volume, and to further avoid a possible crack interpenetration by imposing a minimal distance (1/100 of the box edge dimension) between cracks, although overlapping is technically possible with Salome. To limit the mesh size, the number of cracks was restrained in the range 30 to 60, corresponding to a crack density parameter varying from 0.2 to 0.8. With the available numerical tools, it is possible to generate geometries with crack aspect ratios as low as 1/1000, to be compared with 1/100 in Vasylevskyi et al. [28]. As a consequence, the numerical strain/stress fields within the cracks are probably questionable due to elements whose shape is not well suited for FE simulations.

The meshes were generated from the geometries with automatic softwares plugged in Salome[2], and are composed of tetrahedrons for volumes and triangles for surfaces. A mesh refinement is systematically imposed on the crack surfaces by increasing the surface triangle density, to improve the quality of the simulation results. Note that a node is enforced on these upper and lower crack surfaces at the normal of each crack center, to determine the crack opening from numerical displacements precisely at this point. The meshes are all periodic, so as to be able to work with periodic boundary conditions in the finite element software Cast3M[3]. Note that under these constraints, it proved difficult for the CAD software to generate the geometries using flat spheroids, so instead flat right circular cylinders were used, which made the generation more manageable for the software. The following points thus needed assessment:

- Mesh convergence
- Representativeness of the elementary volumes

[1] https://www.salome-platform.org
[2] http://www.distene.com
[3] http://www-cast3m.cea.fr

- Impact of using right circular cylinders instead of spheroids

The last point was particularly essential because the main original contribution of the present work is the comparison of the crack closure/opening during loading obtained from numerical simulations with that calculated with the homogenization schemes, and the geometry of the inclusions was likely to have an influence. Let us address it first.

In order to determine the effect of the geometry of the inclusions, 2D axisymmetric numerical simulations were first performed, since both spheroids and right circular cylinders possess this symmetry. These simulations consisted in a simple representation of Eshelby's problem of a single inclusion embedded in an isotropic linear elastic medium and subjected to a state of uniaxial tension $\boldsymbol{\Sigma} = \Sigma \boldsymbol{e}_3 \otimes \boldsymbol{e}_3$ far from the inclusion (for numerical simulations, the width and height of the domain were 15 times the radius of the crack). Note that we took advantage of the symmetry of the problem with respect to the mid-plane of the crack and only considered half of the domain, with the symmetry condition on the displacement $\xi_3 = 0$ at the plane of symmetry. The convergence of the resulting crack opening with respect to the aspect ratio of the crack was analyzed for both geometries and compared to Eshelby's analytical result in the limit $X \to 0$. Two different ways of quantifying the crack opening ΔX were tested: the domain occupied by the crack was meshed and given a vanishing Young's modulus with respect to that of the matrix (contrast: $2 \cdot 10^{-11}$) so as to be able to simply average the strain component ε_{33} over the crack, and the displacement ξ_3 at the middle of the crack was also determined. The crack opening ΔX was then calculated from both results. As can be seen from figure 2, averaging the strain component does not yield satisfactory results since the right circular cylinder systematically underestimates the crack opening. Furthermore, convergence of the result as $X \to 0$ is difficult, probably due to the quality of the mesh for X approaching 10^{-3}, although an effort was made to decrease the mesh size as X got smaller. On the other hand, the data from ξ_3 at the middle of the crack is robust in terms of inclusion geometry and converges nicely as $X \to 0$. These results validate the use of right circular cylinders but suggest to analyze crack opening/closure by looking at the relative displacements at the middle of the cracks lips instead of the average strain in the cracks. This means that meshing the inclusions is of no use here and can be avoided. More generally, we could consider more simple alternative representations of the cracks, e.g. by surfaces; this point will be investigated in a future work.

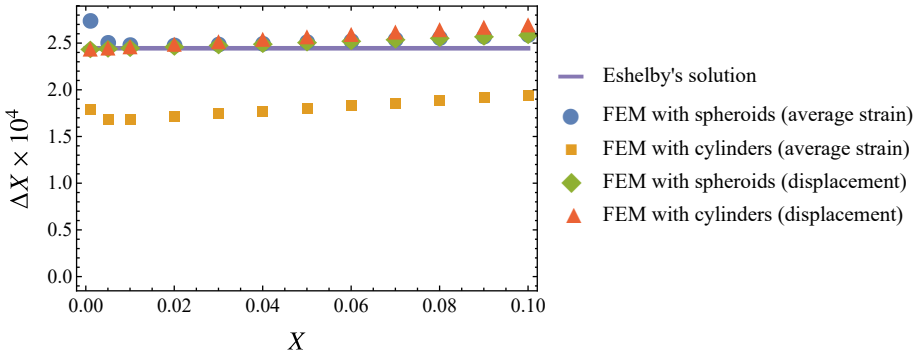

Figure 2: Crack opening assessment: spheroids versus cylinders and strain versus displacement. Here, $\Sigma = 1$MPa and $E = 5$GPa, $\nu = 0.2$ in the matrix.

Additionally, 3D simulations on an actual geometry containing 40 aligned cracks with $X = \frac{1}{1000}$ ($\epsilon = 0.4$) were performed so as to check that these results transpose well to the 3D case. The out-of-plane elastic moduli obtained with the two geometries (spheroidal and cylindrical cracks) were also compared. Since the 3D geometries were generated randomly, they were not perfectly transversely isotropic, however, the deviation from transverse isotropy was very small (see below). Thus, the effective out-of-plane Young's modulus and shear modulus could be directly computed from two simulations with prescribed stress and periodic boundary conditions: one with $\boldsymbol{\Sigma} = \Sigma \boldsymbol{e}_3 \otimes \boldsymbol{e}_3$ and one with $\boldsymbol{\Sigma} = \Sigma(\boldsymbol{e}_1 \otimes \boldsymbol{e}_3 + \boldsymbol{e}_3 \otimes \boldsymbol{e}_1)$. We compared these two effective moduli for identical geometries, i.e. the centroids of the cracks are at the same locations, so that the only difference is the shape of the cracks. We found a relative difference of 0.6% and 0.2% on the effective Young's moduli and shear moduli respectively, and a relative difference of 0.8% on the average values of the crack closure among the 40 cracks. These results allow resorting to cylinders instead of spheroids in the following investigations, the former being easier to work with.

In order to assess the quality of the mesh used, we investigated the convergence of the effective elastic moduli and crack closure with the growing number of elements in the simulation. Since it is the crack tips that require a high number of elements, we ensured convergence on the elementary volume with the greatest number of cracks, namely 60 cracks ($\epsilon = 0.8$). As can be seen from table 1, the third column presents relative errors with respect to the fourth one of only a few percents. However, it took about an hour to perform the computation on the elementary volume with 4.32 million elements while it took about ten hours to perform the one with 6.29 million elements. The quantitative improvement was not worth the computation time, so for convenience, we performed all the other computations with a mesh size comparable to that of the simulation presented in the third column.

Table 1: Mesh convergence study. Parameters are identical to those of figure 2. The relative error with respect to the last column is given in parentheses.

Number of elements $\times 10^{-6}$	0.51	1.83	**4.32**	6.29
E_3/E	0.0718 (35%)	0.0600 (13%)	**0.0550 (3.6%)**	0.0531
μ_{13}/μ	0.253 (13%)	0.237 (5%)	**0.229 (1.8%)**	0.225
$\Delta X \times 10^3$	1.03 (26%)	1.24 (11%)	**1.35 (3%)**	1.39

Finally, let us tackle the representativeness of the elementary volumes. This was done for two values of the crack density, namely $\epsilon = 0.4$ and $\epsilon = 0.8$ and calculations were performed for four types of boundary conditions: periodic stress (PSBC), periodic strain (PEBC), uniform stress (USBC) and uniform strain (UEBC). Technically speaking, the solver implemented in Cast3M in the case of linear elasticity is based on a variational approach, namely the principle of minimum potential energy is applied, under specific constraints related to the boundary conditions. The surface tractions are directly included in the work of external forces, while the prescribed displacements are accounted for using Lagrange multipliers. Thus, the following functionals are stationary

in the case of uniform boundary conditions:

$$\begin{cases} W(\boldsymbol{\xi}') - \boldsymbol{\Sigma} : \int\limits_{\partial\Omega} \boldsymbol{\xi}'(z) \otimes \boldsymbol{n}(z) \, \mathrm{d}S & \text{(USBC)} \\ W(\boldsymbol{\xi}') - \int\limits_{\partial\Omega} \boldsymbol{\lambda}(z) \cdot (\boldsymbol{\xi}'(z) - \boldsymbol{E} \cdot z) \, \mathrm{d}S & \text{(UEBC)} \end{cases} \tag{19}$$

where $\boldsymbol{\xi}'$ is a virtual displacement field, Ω, $\partial\Omega$ and $\boldsymbol{n}(z)$ are respectively the domain, its boundary and its outward unit normal, W is the elastic energy, $\boldsymbol{\Sigma}$ and $\boldsymbol{E}$ are the applied stress and strain tensors respectively, and $\boldsymbol{\lambda}(z)$ represents the Lagrange multipliers. Of course these functionals are discretized in Cast3M, so that a linear system is eventually solved. Note that for uniform strain boundary conditions, the functional is stationary with respect to both the displacement field and the Lagrange multipliers. In the case of periodic boundary conditions, linear relationships between the displacement vectors on the different faces are applied. If l is the length of the side of the cubic simulation box, and assuming that the coordinate axes are chosen so that three faces of the domain correspond to $z_i = 0$ with $i \in \{1, 2, 3\}$, the following functional is stationary in the case of periodic stress boundary conditions:

$$\begin{aligned} W(\boldsymbol{\xi}') - \boldsymbol{\Sigma} : & \int\limits_{\partial\Omega} \boldsymbol{\xi}'(z) \otimes \boldsymbol{n}(z) \, \mathrm{d}S \\ & - \sum_{i=1}^{3} \int\limits_{z_i=0} \boldsymbol{\lambda}(z) \cdot \left\{ [\boldsymbol{\xi}'(z + l\boldsymbol{e}_i) - \boldsymbol{\xi}'(z)] - [\boldsymbol{\xi}'(l\boldsymbol{e}_i) - \boldsymbol{\xi}'(\boldsymbol{0})] \right\} \mathrm{d}S \end{aligned} \tag{20}$$

where $\boldsymbol{e}_i$ is the unit vector along the Oz_i axis. The last term in (20) ensures that the solution is of the form $\boldsymbol{\xi}(z) = \boldsymbol{E} \cdot z + \boldsymbol{\xi}^{per}(z)$, where $\boldsymbol{\xi}^{per}(z)$ is the periodic part of the displacement, without having to specify the value of $\boldsymbol{E}$, since the loading is here controlled *via* the stress tensor. On the other hand, the following functional is stationary in the case of periodic strain boundary conditions:

$$W(\boldsymbol{\xi}') - \sum_{i=1}^{3} \int\limits_{z_i=0} \boldsymbol{\lambda}(z) \cdot \left\{ [\boldsymbol{\xi}'(z + l\boldsymbol{e}_i) - \boldsymbol{\xi}'(z)] - \boldsymbol{E} \cdot z \right\} \mathrm{d}S \tag{21}$$

As in the case of uniform strain boundary conditions, the two functionals (20) and (21) are stationary with respect to both the displacement field and the Lagrange multipliers. Note that formally speaking, (20) and (21) are stationary for the exact same displacement field and Lagrange multipliers if the prescribed average stress and strain tensors are related by $\boldsymbol{\Sigma} = \mathbb{C}^{per} : \boldsymbol{E}$, where $\mathbb{C}^{per}$ is the effective stiffness tensor of the periodic composite. Indeed, $\boldsymbol{\Sigma}$ and $\boldsymbol{E}$ are conjugate variables, and using one or the other is simply a matter of convenience. This is why the strain-based and stress-based periodic boundary conditions should systematically yield the same stiffness tensors. Nonetheless, they were both used here to ensure consistency of the procedures implemented in Cast3M, and so that the desired loading parameter (here the stress tensor) may be applied later on. On the contrary, the two functionals given in (19) have nothing in common in general, and they do yield two different stiffness tensors. However, the discrepancy between the stress-based and strain-based effective stiffness tensors determined with uniform boundary conditions vanishes as the size

of the volume element becomes much larger than the characteristic size of the heterogeneity. They may thus be used to determine whether or not the domain is large enough.

For the four different kinds of boundary conditions, we computed the full effective stiffness tensor, and we first evaluated the departure from transverse isotropy. This was quantified by calculating the distance of the full tensor to the linear subspace of fourth-ranked transversely isotropic tensors with axis of isotropy along $\boldsymbol{e}_3$. The distance was defined according to the dot product on 6×6 matrices using the Mandel representations of the tensors. It can be computed easily since the projection of any symmetric fourth-ranked tensor (with no particular material symmetry) on this subspace is explicitly known as a function of its components, as is shown in Appendix B. Denoting $||\bullet||$ the norm associated to this dot product, and $\Pi(\mathbb{C})$ the projection of $\mathbb{C}$, the relative distance to the linear subspace considered is $\frac{||\mathbb{C}-\Pi(\mathbb{C})||}{||\mathbb{C}||}$. The relative distances obtained are given in table 2. As can be seen, the full tensors are very close to being transversely isotropic. If the effective medium were far from being transversely isotropic, then we could conclude that the elementary volumes were not representative. Note that the converse is not true, which means that although these results are positive, they do not prove the quality of our elementary volumes. However, they do justify the introduction of the five elastic moduli of a transversely isotropic medium (see equation (A.1)). In order to truly quantify the quality of the elementary volumes, the out-of-plane Young's moduli and shear moduli were compared. As expected, the stiffest effective medium is obtained for uniform strain boundary conditions, while the softest is obtained for uniform stress boundary conditions (see table 3). As the size of the elementary volume increases, these lower and upper bounds should theoretically converge towards the same value when the volume is big enough to contain many inclusions. This limit is the actual effective stiffness of the medium. The values reported in table 3 show an important discrepancy between the uniform strain and uniform stress boundary conditions for a given value of ϵ, which suggests that the domain considered is either not big enough compared to the size of the inclusions, or does not contain enough of them. Since the periodic boundary conditions yield intermediate values, these are the boundary conditions that will be considered in the rest of this paper, despite the additional computation time required.

Table 2: Relative distances from the subspace of transversely isotropic tensors for different boundary conditions and crack densities.

ϵ	0.4	0.8
Rel. Dist. (PSBC)	1.5‰	0.9‰
Rel. Dist. (PEBC)	1.5‰	0.9‰
Rel. Dist. (USBC)	0.8‰	0.7‰
Rel. Dist. (UEBC)	1.3‰	1‰

3.2. Results and discussion

We now present the results in terms of out-of-plane Young's modulus (E_3) and shear modulus (μ_{13}), as well as crack opening. The two elastic moduli were systematically determined with periodic boundary conditions with prescribed average stress, since only two simulations are then necessary, as described in section 3.1. Four values of ϵ were considered, namely 0.2, 0.4, 0.6 and

Table 3: Quantitative evaluation of the representativeness of the elementary volumes. E_3, μ_{13}: effective out-of-plane Young's modulus and shear modulus. Parameters are identical to those of figure 2.

ϵ	0.4	0.8	ϵ	0.4	0.8
E_3/E (PSBC)	0.181	0.047	μ_{13}/μ (PSBC)	0.462	0.228
E_3/E (PEBC)	0.181	0.047	μ_{13}/μ (PEBC)	0.462	0.228
E_3/E (USBC)	0.056	0.021	μ_{13}/μ (USBC)	0.340	0.156
E_3/E (UEBC)	0.389	0.170	μ_{13}/μ (UEBC)	0.596	0.390

0.8, with respectively 30, 40, 50 and 60 inclusions. In each case three geometries were generated to investigate the scatter in the data. One such geometry is shown on figure 3 for each value of ϵ.

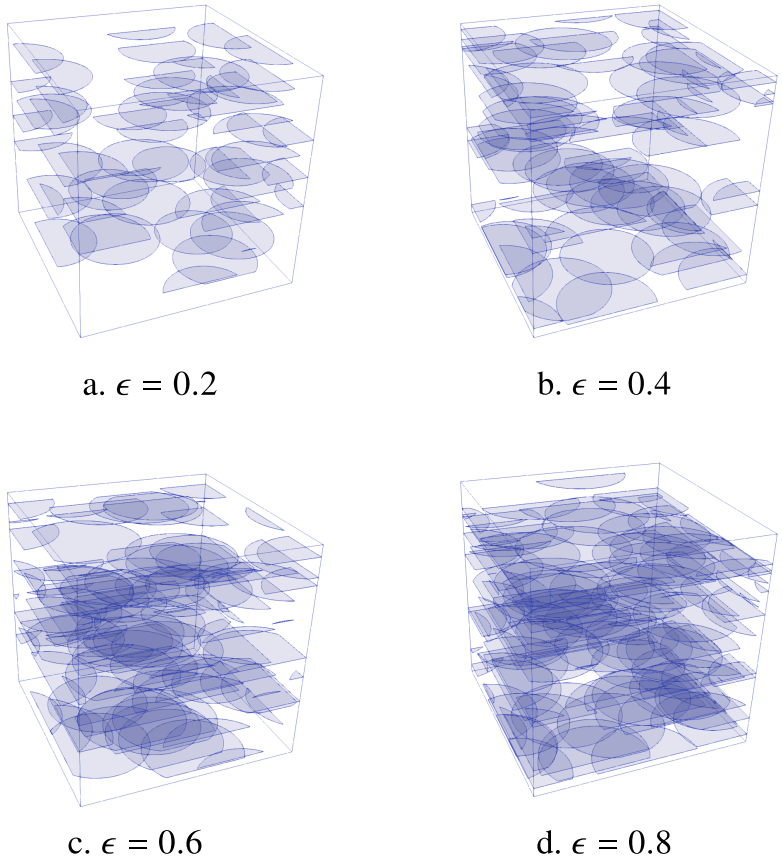

a. $\epsilon = 0.2$ b. $\epsilon = 0.4$

c. $\epsilon = 0.6$ d. $\epsilon = 0.8$

Figure 3: Four periodic geometries generated.

The evolution with respect to ϵ of the effective Young's moduli and shear moduli are shown on figure 4 (symbols) and are compared with the analytical estimates (solid lines). For the numerical simulations, the symbols represent the average values of the moduli over the three simulations for each value of ϵ. The scatter could not be shown in this figure because it is smaller than the size

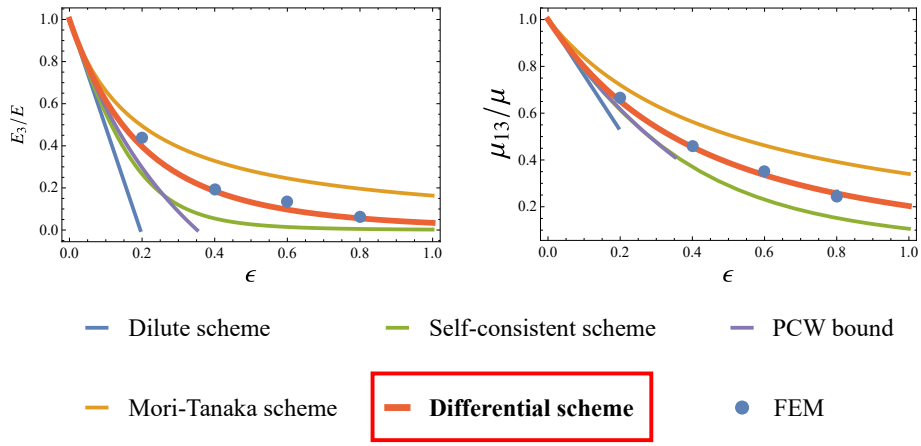

Figure 4: Effective elastic moduli as a function of crack density parameter. Five classical approximations versus numerical simulations.

of the symbol, which is evidence of its small amplitude. As can be seen, the differential scheme is the one that best fits the numerical simulations.

A couple of remarks deserve to be made at this point. First, concerning the fact that a number of authors found the dilute scheme to be the best fit (Zhan et al. [31], Grechka [12]), although it is supposed to neglect interactions between the inclusions, it should be noted that these authors followed Kachanov [19] and used stress-based estimates of the elastic moduli. The stress-based dilute estimate of the compliance tensor is indeed given by (9), which directly yields:

$$\frac{E}{E_3^{hom}} \sim 1 + \frac{16}{3}(1-\nu^2)\epsilon \tag{22}$$

Given this result, it is tempting to then write $E_3^{hom} \sim E\left(1+\frac{16}{3}(1-\nu^2)\epsilon\right)^{-1}$, as the previously mentioned works did, without considering low crack densities. However, since the dilute estimate is only relevant to first order in ϵ, one should take the expansion up to first order in ϵ of the previous formula, which yields (10). The same logic applies to the out-of-plane shear modulus. As explained in Dormieux and Kondo [10], one should be careful when using the dilute approximation, because the stress-based dilute estimate of the compliance tensor is not rigorously the inverse of the strain-based dilute estimate of the stiffness tensor. In fact, one can show that $\mathbb{S}^{dil} : \mathbb{C}^{dil} - \mathbb{I}$ is of the order of ϵ^2, where $\mathbb{I}$ is the fourth-rank identity tensor. Thus, the previously mentioned authors actually used the Mori-Tanaka estimate instead of the dilute estimate.

Secondly, it is important to consider the distribution of the cracks and how it relates to the status of the PCW bound with respect to the present numerical results. In the present study, the crack centroids were positioned randomly in the elementary volumes, but because of the flatness of the cracks the statistical distribution of the crack phase is not isotropic. On the contrary, since the width of the cracks is much larger than their thickness and the centroids are equally spaced on average in all directions, the distances between the cracks are much lower in the $(\boldsymbol{e}_1, \boldsymbol{e}_2)$ plane than in the $\boldsymbol{e}_3$ direction. Moreover, the geometries and the boundary conditions applied here are periodic, which means that the associated two-point correlation functions are also periodic. As a

consequence, the hypotheses of ellipsoidal symmetry and of no long-range order, which are central to the analysis proposed in Ponte Castaneda and Willis [24], do not hold. The PCW bounds are therefore not rigorous bounds for the effective properties determined numerically in this work, which is why they are not respected in figure 4. Of course, the generated samples have a certain spatial distribution of cracks which results from the random positions of the centroids, but it is not so easily characterized, and one should keep in mind that the differential scheme is the best fit for this particular spatial distribution. Taking another distribution would most likely lead to a different result, so that it would be necessary to investigate the kind of distribution that is actually observed on cracked samples.

Figure 5 shows the crack openings when the elementary volume is subjected to a uniaxial tension of 1MPa. Again, there is very good agreement between the numerical results and the differential scheme. However, the scatter in the average values per simulation is much greater than for the elastic moduli, especially for $\epsilon = 0.8$, and can here be seen. The scatter is indeed represented by the maximum (top of the symbol), minimum (bottom of the symbol) and average (central dot) values of the three simulations. This could have been expected since the moduli are macroscopic averages over the whole simulation cell while the crack opening is a very local information. Indeed, recall that the latter is estimated through the displacements of two opposite points of the crack lips, which may bias the results in case of strong crack-to-crack interaction. A direct consequence is that more realizations of samples should probably be generated and with more cracks so as to have a better characterization of this spread.

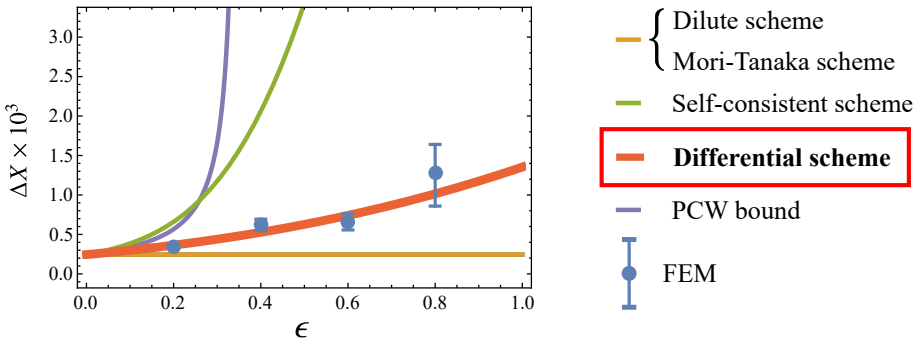

Figure 5: Crack opening as a function of crack density parameter for a 1MPa uniaxial tension. Five classical approximations versus numerical simulations.

Still, with the data already collected, we were able to look more closely at the statistical distribution of ΔX on the different simulations. Indeed, the values shown are the average values per simulation, but there is also scatter in each one of them, as can be seen from figures 6 and 7, where a smooth histogram is shown from combining all the simulations in the case $\epsilon = 0.2$ and $\epsilon = 0.8$ respectively, and vertical straight lines represent the predictions of the homogenization schemes. The predictions of the self-consistent scheme are not included because they are out of the plotted ranges. The two figures are quite different, since for $\epsilon = 0.2$ the distribution is rather symmetric about its mean, while it is right-skewed for $\epsilon = 0.8$. As was to be expected from figure 5, the prediction of the differential scheme is slightly above the average value for $\epsilon = 0.2$ and slightly below for $\epsilon = 0.8$, so that this scheme neither overestimates nor underestimates crack

closure consistently. The spread in the distributions shown suggests that the hypothesis made in Deude et al. [8] that all the cracks close simultaneously in the non-linear model during compression should be further investigated on an actual non-linear simulation.

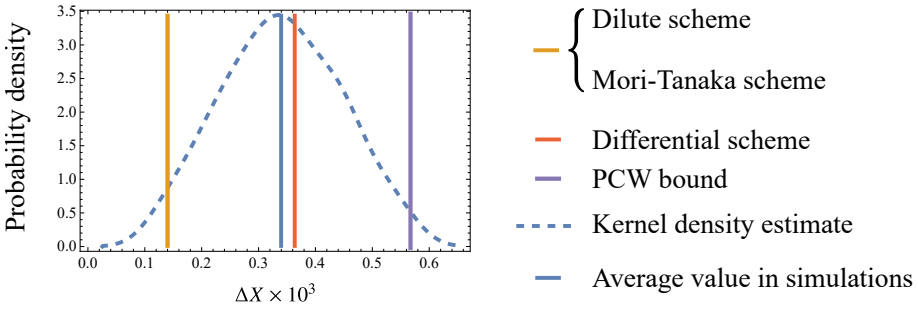

Figure 6: Crack opening distribution over the three simulations with $\epsilon = 0.2$.

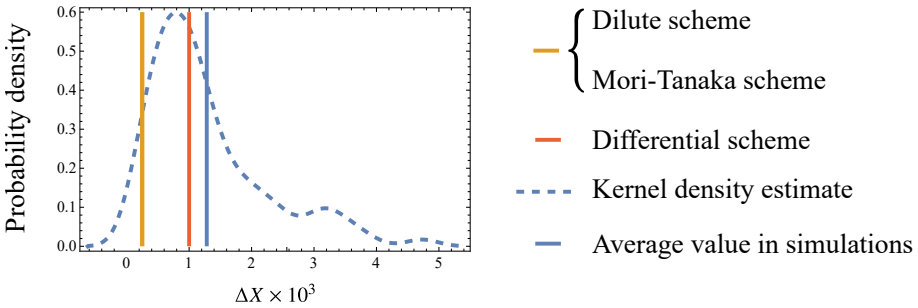

Figure 7: Crack opening distribution over the three simulations with $\epsilon = 0.8$.

4. Conclusion

Deude et al. [8] proposed a non-linear micromechanical model of cracked media that takes into account complete crack closure. This approach was initially restricted to the Mori-Tanaka scheme, probably for convenience since its implementation only requires computation of the Hill tensor of a crack in an isotropic matrix. The non-linearity hinges on the computation of the closure of the cracks, which thus needs to be accurate enough not to overestimate/underestimate the stiffness of the material. Until now, the confrontation between the different micromechanical schemes and numerical simulations had focused exclusively on the effective stiffness that they predict, and not on the strain concentration in the cracks, so that it was difficult to assess how realistic the non-linear model of Deude et al. [8] was. The aim of this paper was precisely to shed light on this.

We focused here on five classical micromechanical estimates: the dilute, Mori-Tanaka, self-consistent and differential schemes and the PCW bounds (section 2). Direct application of these schemes to cracked media shows that they differ in terms of both stiffness and strain concentration. The Mori-Tanaka and self-consistent schemes are the stiffest and softest respectively, and the dilute and Mori-Tanaka schemes have the particular feature that the crack closure does not depend on

the crack density but only on the stiffness of the solid matrix and the mechanical load. It is thus tempting to think that these schemes will underestimate the actual crack closure.

Numerical simulations were performed using the finite element software Cast3M to investigate the validity of these results (section 3). Several periodic geometries were generated at different crack densities from 0.2 to 0.8, and were subjected to periodic boundary conditions. Consistency of the geometrical representation of the cracks was ensured by comparing different shapes with small aspect ratios, and the representativeness of the simulation box was investigated. The results show that both out-of-plane effective elastic moduli are very well predicted by the differential scheme, which confirms previous results of the literature (Dahm and Becker [7], Orlowsky et al. [23], Shen and Li [27], Vasylevskyi et al. [28]). A new interesting result obtained in the present study is that this scheme is also very good at predicting the average crack opening. These results suggest that the differential scheme should be preferred to estimate both the out-of-plane moduli and crack closure of a cracked medium with parallel cracks over the Mori-Tanaka scheme, which means that it is also better suited for a non-linear model. However, it should be stressed that the nature of the sample generation process determines the spatial distribution of the phases. The present result thus only holds for randomly placed crack centroids, and actual spatial distribution in cracked media should be investigated in order to confront the present results to real geometries.

As noted in section 3.1, we have shown that it is more relevant to measure the crack aperture variation from displacements at the middle of the cracks than from the average strain in the volume of the cracks. One way to improve on our simulations would thus be to dispense with meshing the interior of the cracks, and even with giving the cracks a finite volume. Indeed, it would actually be easier to simply consider the cracks as perfectly flat, that is, as two initially coinciding surfaces which are free of surface tractions. In that case, one could contemplate using XFEM to perform the computations, since this technique can deal with such geometries. These improvements might allow us to deal with higher numbers of cracks in the simulations, which in turn should lead to more accurate results, given the difference observed here between uniform stress and uniform strain boundary conditions.

Finally, we have discussed the presence of a crack opening distribution within the simulations. This suggests that working with only its average value in a non-linear model might be insufficient, since there will exist a range of loads for which some cracks are closed and some are open. It would thus be interesting to perform non-linear numerical experiments whereby contact between the crack faces is accounted for, either explicitly if the cracks are given a finite volume, or through a fictitious non-linear spring between the crack surfaces if they are perfectly flat, as suggested above. This spring should have a negligible stiffness as long as the displacement jump does not exceed a specified value, and a very large one when this value is reached. Comparison with the non-linear analytical model whereby all the cracks close simultaneously would allow to conclude on the importance of this phenomenon. The difficulty may lie in the fact that it is not guaranteed that periodic boundary conditions lead to existence and uniqueness of the solution in this non-linear context. If uniform strain/stress boundary conditions are used instead, much larger unit cells have to be used, so that the upper and lower bounds given by the uniform strain and uniform stress boundary conditions be relatively close to each other, which could make the computation cost prohibitive.

Appendix A. Concentration tensor for a flat spheroid in a transversely isotropic matrix

Let $\mathscr{B} = (\boldsymbol{e}_1, \boldsymbol{e}_2, \boldsymbol{e}_3)$ be an orthonormal basis of the Euclidean space. Let $\mathbb{C}^0$ be the stiffness tensor of a transversely isotropic linear elastic medium with its axis of transverse isotropy parallel to $\boldsymbol{e}_3$. We will use the Mandel representation of second-rank and fourth-rank symmetric tensors, that is, both stress and strain tensors are represented by (6×1) column vectors denoted $[\boldsymbol{\alpha}]_{\mathscr{B}}$ using their components in $\mathscr{B}$ with the convention $[\boldsymbol{\alpha}]_{\mathscr{B}} = \left(\alpha_{11}, \alpha_{22}, \alpha_{33}, \sqrt{2}\alpha_{23}, \sqrt{2}\alpha_{13}, \sqrt{2}\alpha_{12}\right)^T$, where $()^T$ denotes the transpose of a row vector. The representation of fourth-rank symmetric tensors follows directly from the convention for second-rank symmetric tensors, so that both stiffness and compliance tensors have the same $\sqrt{2}$ and 2 factors in their representations. Then, following Hoenig [15], the representation of the compliance tensor $\mathbb{S}^0$ reads:

$$[\mathbb{S}^0]_{\mathscr{B}} = \frac{1}{E}\begin{pmatrix} 1 & -\nu_1 & -\nu_2 & 0 & 0 & 0 \\ -\nu_1 & 1 & -\nu_2 & 0 & 0 & 0 \\ -\nu_2 & -\nu_2 & \frac{1}{H} & 0 & 0 & 0 \\ 0 & 0 & 0 & \frac{1+\nu_1}{\Gamma} & 0 & 0 \\ 0 & 0 & 0 & 0 & \frac{1+\nu_1}{\Gamma} & 0 \\ 0 & 0 & 0 & 0 & 0 & 1+\nu_1 \end{pmatrix} \tag{A.1}$$

The representation of the tensor $\mathbb{U}^{c,0}$ for a circular crack with unit normal $\boldsymbol{e}_3$ can then be deduced from Hoenig [15]:

$$[\mathbb{U}^{c,0}]_{\mathscr{B}} = \begin{pmatrix} 0 & 0 & 0 & 0 & 0 & 0 \\ 0 & 0 & 0 & 0 & 0 & 0 \\ 0 & 0 & A & 0 & 0 & 0 \\ 0 & 0 & 0 & B & 0 & 0 \\ 0 & 0 & 0 & 0 & B & 0 \\ 0 & 0 & 0 & 0 & 0 & 0 \end{pmatrix} \tag{A.2}$$

with:

$$\begin{cases} A = \frac{4}{\pi}\frac{1}{E}S\sqrt{\frac{\frac{1}{H}-\nu_2^2}{1-\nu_1^2}} \\ B = \frac{4}{\pi}\frac{1}{E}\frac{S}{1+\frac{S}{T}} \end{cases} \tag{A.3}$$

where S and T are given by:

$$\begin{cases} S = \sqrt{\frac{1-\nu_1^2}{2}}\sqrt{(1+\nu_1)\left(\frac{1}{\Gamma}-\nu_2\right) + \sqrt{(1-\nu_1^2)\left(\frac{1}{H}-\nu_2^2\right)}} \\ T = \frac{1+\nu_1}{\sqrt{\Gamma}} \end{cases} \tag{A.4}$$

Note that we have corrected the missing parentheses in the expression for S as found in Hoenig [15]. In the isotropic case, $\nu_1 = \nu_2 = \nu$ and $H = \Gamma = 1$, so that $S = 1 - \nu^2$ and $T = 1 + \nu$ and:

$$\begin{cases} A = \frac{4}{\pi}\frac{1-\nu^2}{E} \\ B = \frac{4}{\pi}\frac{1-\nu^2}{(2-\nu)E} \end{cases} \tag{A.5}$$

Appendix B. Projection on the linear subspace of transversely isotropic fourth-ranked tensors

Let $\mathscr{W} = (\mathbb{E}^1, \mathbb{E}^2, \mathbb{E}^3, \mathbb{E}^4, \mathbb{F}, \mathbb{G})$ be the basis of the linear space of transversely isotropic tensors with $\boldsymbol{n}$ as axis of transverse isotropy defined in Walpole [30]. According to their definitions, in any orthonormal basis $\mathscr{B} = (\boldsymbol{e}_1, \boldsymbol{e}_2, \boldsymbol{e}_3)$ such that $\boldsymbol{e}_3 = \boldsymbol{n}$, they have the following Mandel representations:

$$[\mathbb{E}^1]_{\mathscr{B}} = \begin{pmatrix} 0 & 0 & 0 & 0 & 0 & 0 \\ 0 & 0 & 0 & 0 & 0 & 0 \\ 0 & 0 & 1 & 0 & 0 & 0 \\ 0 & 0 & 0 & 0 & 0 & 0 \\ 0 & 0 & 0 & 0 & 0 & 0 \\ 0 & 0 & 0 & 0 & 0 & 0 \end{pmatrix}; \quad [\mathbb{E}^2]_{\mathscr{B}} = \begin{pmatrix} \frac{1}{2} & \frac{1}{2} & 0 & 0 & 0 & 0 \\ \frac{1}{2} & \frac{1}{2} & 0 & 0 & 0 & 0 \\ 0 & 0 & 0 & 0 & 0 & 0 \\ 0 & 0 & 0 & 0 & 0 & 0 \\ 0 & 0 & 0 & 0 & 0 & 0 \\ 0 & 0 & 0 & 0 & 0 & 0 \end{pmatrix}; \quad [\mathbb{E}^3]_{\mathscr{B}} = \begin{pmatrix} 0 & 0 & 0 & 0 & 0 & 0 \\ 0 & 0 & 0 & 0 & 0 & 0 \\ \frac{1}{\sqrt{2}} & \frac{1}{\sqrt{2}} & 0 & 0 & 0 & 0 \\ 0 & 0 & 0 & 0 & 0 & 0 \\ 0 & 0 & 0 & 0 & 0 & 0 \\ 0 & 0 & 0 & 0 & 0 & 0 \end{pmatrix}$$

$$[\mathbb{E}^4]_{\mathscr{B}} = \begin{pmatrix} 0 & 0 & \frac{1}{\sqrt{2}} & 0 & 0 & 0 \\ 0 & 0 & \frac{1}{\sqrt{2}} & 0 & 0 & 0 \\ 0 & 0 & 0 & 0 & 0 & 0 \\ 0 & 0 & 0 & 0 & 0 & 0 \\ 0 & 0 & 0 & 0 & 0 & 0 \\ 0 & 0 & 0 & 0 & 0 & 0 \end{pmatrix}; \quad [\mathbb{F}]_{\mathscr{B}} = \begin{pmatrix} \frac{1}{2} & -\frac{1}{2} & 0 & 0 & 0 & 0 \\ -\frac{1}{2} & \frac{1}{2} & 0 & 0 & 0 & 0 \\ 0 & 0 & 0 & 0 & 0 & 0 \\ 0 & 0 & 0 & 0 & 0 & 0 \\ 0 & 0 & 0 & 0 & 0 & 0 \\ 0 & 0 & 0 & 0 & 0 & 1 \end{pmatrix}; \quad [\mathbb{G}]_{\mathscr{B}} = \begin{pmatrix} 0 & 0 & 0 & 0 & 0 & 0 \\ 0 & 0 & 0 & 0 & 0 & 0 \\ 0 & 0 & 0 & 0 & 0 & 0 \\ 0 & 0 & 0 & 1 & 0 & 0 \\ 0 & 0 & 0 & 0 & 1 & 0 \\ 0 & 0 & 0 & 0 & 0 & 0 \end{pmatrix} \tag{B.1}$$

Note that $\mathbb{E}^3$ and $\mathbb{E}^4$ are unsymmetric. The rules of multiplication between these tensors are easily recovered using matrix multiplications on these representations. The dot product defined on (6×6) matrices is $\mathrm{Tr}\left(A^T B\right)$, where A and B are two such matrices, A^T is the transpose of A and $\mathrm{Tr}(\bullet)$ is the trace operator. This dot product is actually simply equal to $\mathbb{A}^T :: \mathbb{B}$, where $\mathbb{A}$ and $\mathbb{B}$ are the two unsymmetric fourth-ranked tensors associated to A and B, and :: is the quadruple contraction of tensors defined as:

$$\mathbb{A} :: \mathbb{B} = A_{ijkl} B_{lkji} \tag{B.2}$$

where Einstein's summation convention on repeated indices was used. Note that all the fourth-ranked tensors considered here possess the minor symmetries (i.e. $A_{ijkl} = A_{jikl} = A_{ijlk}$), so that they do have a Mandel representation, and the words "symmetric" and "unsymmetric" only refer to the major symmetry ($A_{ijkl} = A_{klij}$). The transpose of $\mathbb{A}$ is thus to be understood as the tensor

whose components are A_{klij}. Its Mandel representation is obviously the transpose of the Mandel representation of $\mathbb{A}$.

Using these rules, it is straightforward to show that $\mathscr{W}$ is orthogonal, but it is not orthonormal, since $\mathbb{F} :: \mathbb{F} = \mathbb{G} :: \mathbb{G} = 2$. An orthonormal basis of the linear subspace of transversely isotropic symmetric tensors can easily be obtained:

$$\mathscr{W}' = (\mathbb{E}^1, \mathbb{E}^2, \frac{1}{\sqrt{2}}\left(\mathbb{E}^3 + \mathbb{E}^4\right), \frac{1}{\sqrt{2}}\mathbb{F}, \frac{1}{\sqrt{2}}\mathbb{G}) \tag{B.3}$$

Since this basis is orthonormal, the orthogonal projection of any fourth-ranked symmetric tensor on the subspace of transversely isotropic tensors is obtained by taking its dot product with the five tensors of the basis. The components of the projection $\Pi(\mathbb{C})$ in $\mathscr{W}'$ are:

$$\begin{cases} a = C_{3333} \\ b = \frac{1}{2}\left(C_{1111} + 2C_{1122} + C_{2222}\right) \\ c = C_{1133} + C_{2233} \\ f = \frac{1}{\sqrt{2}}\left(\frac{C_{1111}+C_{2222}}{2} - C_{1122} + 2C_{1212}\right) \\ g = \sqrt{2}\left(C_{2323} + C_{1313}\right) \end{cases} \tag{B.4}$$

and the more classically used components follow:

$$\begin{cases} \Pi(\mathbb{C})_{1111} = \frac{1}{4}\left(3\frac{C_{1111}+C_{2222}}{2} + C_{1122} + 2C_{1212}\right) \\ \Pi(\mathbb{C})_{1122} = \frac{1}{4}\left(\frac{C_{1111}+C_{2222}}{2} + 3C_{1122} - 2C_{1212}\right) \\ \Pi(\mathbb{C})_{1133} = \frac{C_{1133}+C_{2233}}{2} \\ \Pi(\mathbb{C})_{3333} = C_{3333} \\ \Pi(\mathbb{C})_{2323} = \frac{C_{1313}+C_{2323}}{2} \end{cases} \tag{B.5}$$

It is easily seen that if $\mathbb{C}$ is transversely isotropic with $\boldsymbol{e}_3$ as axis of transverse isotropy, then the original components of $\mathbb{C}$ are recovered in (B.5), since we then have $C_{1111} = C_{2222}$, $C_{1133} = C_{2233}$, $C_{1313} = C_{2323}$ and $2C_{1212} = C_{1111} - C_{1122}$.

Acknowledgment

The authors gratefully acknowledge financial support from CEA and EDF/ERMES.

References

[1] J.-F. Barthélémy. Effective permeability of media with a dense network of long and micro fractures. *Transport in porous media*, 76(1):153–178, 2009. URL `http://www.springerlink.com/index/92x601894jv33520.pdf`.

[2] B. Bary, M. Ben Haha, E. Adam, and P. Montarnal. Numerical and analytical effective elastic properties of degraded cement pastes. *Cement and Concrete Research*, 39(10):902–912, oct 2009. doi: 10.1016/j.cemconres.2009.06.012.

[3] B. Bary, C. Bourcier, and T. Helfer. Analytical and 3d numerical analysis of the thermoviscoelastic behavior of concrete-like materials including interfaces. *Advances in Engineering Software*, 112:16–30, oct 2017. doi: 10.1016/j.advengsoft.2017.06.006.

[4] J. Bluthé, B. Bary, and E. Lemarchand. Micromechanical modeling of the Compression of the Damaged Zone experiment in the Callovo-Oxfordian formation. *Advances in Geosciences*, 45:25–33, jul 2018. doi: 10.5194/adgeo-45-25-2018.

[5] B. Budiansky and R. J. O'connell. Elastic moduli of a cracked solid. *International journal of Solids and structures*, 12(2):81–97, 1976.

[6] L. Charpin and A. Ehrlacher. Estimating the poroelastic properties of cracked materials. *Acta Mechanica*, 225(9):2501–2519, September 2014. ISSN 1619-6937. doi: 10.1007/s00707-013-1082-0. URL https://doi.org/10.1007/s00707-013-1082-0.

[7] T. Dahm and T. Becker. On the elastic and viscous properties of media containing strongly interacting in-plane cracks. *Pure and Applied Geophysics*, 151(1):1–16, jan 1998. doi: 10.1007/s000240050102.

[8] V. Deude, L. Dormieux, D. Kondo, and S. Maghous. Micromechanical approach to nonlinear poroelasticity: application to cracked rocks. *Journal of engineering mechanics*, 128(8):848–855, 2002. URL http://ascelibrary.org/doi/abs/10.1061/(ASCE)0733-9399(2002)128:8(848).

[9] L. Dormieux and D. Kondo. Approche micromécanique du couplage perméabilité–endommagement. *Comptes Rendus Mécanique*, 332(2):135–140, 2004.

[10] L. Dormieux and D. Kondo. *Micromechanics of Fracture and Damage*. John Wiley & Sons, 2016.

[11] J. D. Eshelby. The Determination of the Elastic Field of an Ellipsoidal Inclusion, and Related Problems. *Proceedings of the Royal Society of London A: Mathematical, Physical and Engineering Sciences*, 241(1226):376–396, August 1957. ISSN 1364-5021, 1471-2946. doi: 10.1098/rspa.1957.0133. URL http://rspa.royalsocietypublishing.org/content/241/1226/376.

[12] V. Grechka. Comparison of the non-interaction and differential schemes in predicting the effective elastic properties of fractured media. *International Journal of Fracture*, 144(3):181–188, jul 2007. doi: 10.1007/s10704-007-9088-z.

[13] Z. Hashin. The differential scheme and its application to cracked materials. *Journal of the Mechanics and Physics of Solids*, 36(6):719–734, January 1988. ISSN 0022-5096. doi: 10.1016/0022-5096(88)90005-1. URL http://www.sciencedirect.com/science/article/pii/0022509688900051.

[14] R. Hill. A self-consistent mechanics of composite materials. *Journal of the Mechanics and Physics of Solids*, 13(4):213–222, August 1965. ISSN 0022-5096. doi: 10.1016/0022-5096(65)90010-4. URL http://www.sciencedirect.com/science/article/pii/0022509665900104.

[15] A. Hoenig. The behavior of a flat elliptical crack in an anisotropic elastic body. *International Journal of Solids and Structures*, 14(11):925–934, January 1978. ISSN 0020-7683. doi: 10.1016/0020-7683(78)90068-9. URL http://www.sciencedirect.com/science/article/pii/0020768378900689.

[16] T. Honorio, B. Bary, and F. Benboudjema. Multiscale estimation of ageing viscoelastic properties of cement-based materials: A combined analytical and numerical approach to estimate the behaviour at early age. *Cement and Concrete Research*, 85:137–155, jul 2016. doi: 10.1016/j.cemconres.2016.03.010.

[17] Y. Huang, A. Chandra, Z. Q. Jiang, X. Wei, and K. X. Hu. The numerical calculation of two-dimensional effective moduli for microcracked solids. *International Journal of Solids and Structures*, 33(11):1575–1586, May 1996. ISSN 0020-7683. doi: 10.1016/0020-7683(95)00110-7. URL http://www.sciencedirect.com/science/article/pii/0020768395001107.

[18] M. Kachanov. Elastic solids with many cracks: A simple method of analysis. *International Journal of Solids and Structures*, 23(1):23–43, 1987. doi: 10.1016/0020-7683(87)90030-8.

[19] M. Kachanov. Effective elastic properties of cracked solids: Critical review of some basic concepts. *Applied Mechanics Reviews*, 45(8):304, 1992. doi: 10.1115/1.3119761.

[20] E. Lemarchand, C. A. Davy, L. Dormieux, W. Chen, and F. Skoczylas. Micromechanics contribution to coupled transport and mechanical properties of fractured geomaterials. *Transport in Porous Media*, 79(3):335–358, jan 2009. doi: 10.1007/s11242-008-9326-5.

[21] E. Lemarchand, C. A. Davy, L. Dormieux, and F. Skoczylas. Tortuosity effects in coupled advective transport and mechanical properties of fractured geomaterials. *Transport in Porous Media*, 84(1):1–19, oct 2009. doi:

10.1007/s11242-009-9481-3.

[22] S. Levasseur, F. Collin, R. Charlier, and D Kondo. A micro–macro approach of permeability evolution in rocks excavation damaged zones. *Computers and Geotechnics*, 49:245–252, 2013.

[23] B. Orlowsky, E. H. Saenger, Y. Guéguen, and S.A. Shapiro. Effects of parallel crack distributions on effective elastic properties - a numerical study. *International Journal of Fracture*, 124(3/4):L171–L178, dec 2003. doi: 10.1023/b:frac.0000022563.29991.80.

[24] P. Ponte Castaneda and J. R. Willis. The effect of spatial distribution on the effective behavior of composite materials and cracked media. *Journal of the Mechanics and Physics of Solids*, 43(12):1919–1951, dec 1995. doi: 10.1016/0022-5096(95)00058-q.

[25] E. H. Saenger, O. S. Kruge, and Shapiro S. A. Effective elastic properties of randomly fractured soils: 3d numerical experiments. *Geophysical Prospecting*, 52(3):183–195, may 2004. doi: 10.1111/j.1365-2478.2004.00407.x.

[26] E. H. Saenger, O. S. Kruge, and Shapiro S. A. Effective elastic properties of fractured rocks: Dynamic vs. static considerations. In *SEG Technical Program Expanded Abstracts 2006*. Society of Exploration Geophysicists, jan 2006. doi: 10.1190/1.2369912.

[27] L. Shen and J. Li. A numerical simulation for effective elastic moduli of plates with various distributions and sizes of cracks. *International Journal of Solids and Structures*, 41(26): 7471–7492, December 2004. ISSN 0020-7683. doi: 10.1016/j.ijsolstr.2004.02.016. URL http://www.sciencedirect.com/science/article/pii/S0020768304000721.

[28] K. Vasylevskyi, B. Drach, and I. Tsukrov. On micromechanical modeling of orthotropic solids with parallel cracks. *International Journal of Solids and Structures*, 144-145:46–58, July 2018. ISSN 0020-7683. doi: 10.1016/j.ijsolstr.2018.02.038. URL http://www.sciencedirect.com/science/article/pii/S0020768318300544.

[29] M.N. Vu, S.T. Nguyen, Q.D. To, and N.H. Dao. Theoretical predicting of permeability evolution in damaged rock under compressive stress. *Geophysical Journal International*, mar 2017. doi: 10.1093/gji/ggx094.

[30] L. J. Walpole. Fourth-rank tensors of the thirty-two crystal classes: multiplication tables. *Proc. R. Soc. Lond. A*, 391(1800):149–179, 1984.

[31] S. Zhan, Z. Wang, and X. Han. Effective elastic moduli of two-dimensional solids with multiple cracks. *Science in China Series A: Mathematics*, 41(10):1114–1120, oct 1998. doi: 10.1007/bf02871847.

[32] Q.-S. Zheng and D.-X. Du. An explicit and universally applicable estimate for the effective properties of multiphase composites which accounts for inclusion distribution. *Journal of the Mechanics and Physics of Solids*, 49(11):2765–2788, 2001. URL http://www.sciencedirect.com/science/article/pii/S0022509601000783.